

# Theoretical and Experimental Study of the Intake Manifold Effect on the SI Engine Performance

Assist. Prof. Dr. Qais A. Rishack  
*Department of Mechanical Engineering  
 University of Basrah  
 College of Engineering*

Assist. Prof. Dr. Sadoun F. Dakhil  
*Department of Mechanical Engineering  
 University of Basrah  
 College of Engineering*

Mohammed K. Obaid  
*Department of Mechanical Engineering  
 University of Basrah  
 College of Engineering*

**Abstract-** This work uses different shapes of intake manifold for study the effect on a single cylinder four stroke gasoline engine. A numerical simulation of the flow achieved through five intake manifold designs, using 3D Computational Fluid Dynamic (CFD) software package FLUENT (6.3.). Accordingly, the three-dimensional resolution of Navier-Stokes equations in conjunction with the standard k- $\epsilon$  turbulence model is undertaken to provide knowledge of the air movement nature and examining the intake manifold optimal geometry. Five cases of intake manifold are examined experimentally in order to produce a comprehensive and realistic data set. These data are in the form of engine performance, exhaust gas products and relative AFR for each case separately under different engine speeds. Exhaust gas analyzer type (Infragas-209) is used in the present work to measure exhaust gas concentrations and relative air/fuel ratio ( $\lambda$ ). The results were obtained in this investigation showed that a Simulate numerically and experimentally is capable to select the optimized intake system geometry with reliability. Velocity is highest near the outer wall at increased the curvature ratio and pressure is highest near the inner wall at increased the curvature ratio. The secondary flow increases when the engine speeds and curvature ratio increase because of increasing the pressure difference between the inner wall and the outer wall. The effect of these parameters explained on the swirl air movement and tumble inside the cylinder are increasing by increase the engine speed and  $\gamma$  respectively. The increasing in the engine speed and the optimum selection of the manifold which designed enhanced the mixing of the fuel with air. The results showed that the optimized manifold 135°- NE (case 5) due to enhance AFR, fuel consumption and exhaust emissions are improved.

## I. Introduction

The main task of an Inlet Manifold (IM) is to distribute air inside the manifold runner uniformly, which is essential for an optimized IM design. The IM design has strong influence on the volumetric efficiency of the engine. An uneven air distribution leads to less volumetric efficiency, power loss and increase of fuel consumption [1]. Increasingly stringent legislation aimed at reducing pollutant emissions from vehicles has intensified efforts to gain better understanding of the various processes involved in internal combustion (IC) engines [2]. This mixture circulates to the intake port through a very complicated path including the air cleaner, intake pipe, and intake manifold. Hence, the design of the intake manifold is an important factor which determines the engine performance. An intake manifold is one of the primary components regarding the performance of an internal combustion engine [3]. The flow characteristics inside the intake manifold and cylinder have been widely studied in the technical literature. Mark et, al. (2006) [4] used of an intake restrictor to limit performance, keep costs low, and maintain a safe racing experience, Initial results were encouraging, but were very sensitive to

geometry. An additional coupled simulation considered the effect of swirl vanes placed upstream of the restrictor throat. Swirl vanes had little to no effect on the performance of the intake. Ramasamy et, al. (2010) [5] optimized the geometry of an intake system in automobile industry to reduce the pressure drop and enhance the filter utilization area by added guide vane, The CFD analysis of the optimized model was again carried out and the results showed good improvement in flow behavior. Hongjiang (2010) [6] improved the performance of engine type 16V240ZJB diesel engine, the method of steady flow test and CFD numerical simulation was adopted to do intake port structure optimization study, The research showed that CFD simulation is an efficient way to design engine intake port. Jianqin (2011) [7] proposed a new method for designing and studying engine intake system based on the technology of CAD/CAE/CFD integration, The study results have provided guidance for designing intake system of engine. Liu (2011) [8] used AVL-FIRE software to do CFD analog computation for the intake port of engine type 168F, he studied the relationship between the intake port structure and velocity field, and found that the bend intersection's structure is the key effect for the flow characteristics of the intake port. Wes et, al. (2010) [9] studied the influence of inlet mixture temperature on the spark ignition engine performance and exhaust emissions, the mean results of investigation are Increasing inlet mixture temperature from (20-50) °C improve in the fuel consumption and the thermal efficiency about (16% and 14%) consecutively and Regarding the exhaust emissions the results showed that the concentration of (CO, HC& NO<sub>x</sub>) decreased about (1.5%,17%,%12.5) consecutively with increasing inlet mixture temperature from (20-50) °C.

### 1.1. The Aim Of The Present Work

The objectives of the present work are to

- 1- Provide significant study of numerical techniques for the flows inside an engine manifold duct and cylinder by using finite volume method.
- 2- Use FLUENT code to examine the effects of the flow characteristics at different engine speeds (Dean numbers) also at different curvature ratio.
- 3- Study the behavior of each engine performance parameters, exhaust gas parameters and  $\lambda$ . At different engine speeds at (1000, 1500, 2000, 2500, 3000 and 3500 RPM) and Cr =10, for five manifold shapes.
- 4- Examine the optimal geometry intake manifold with experiments tests which are carried out to identify the manifold design effect on the engine performance and the exhaust gases with different engine speeds.

5- Investigate the effect of manifold shape on the fuel mixture characteristics, the engine performance and the exhaust emissions.

## 2. Intake Manifolds Considerations

The studied model is a SI engine gasoline. For this current design of manifold were considered to study the flow and mixture behavior. The design an optimal intake manifold, following parameters were be taken into consideration [2].

- 1- Uniform distribution of mixture to all cylinders.
- 2- Minimum possible resistance in runners.
- 3- To assist fuel atomization and vaporization by swirl flow inside combustion chamber.
- 4- To provide equal aspiration intervals between the branch pipes.

### 2.1 The Physical Model And Parameters Definitions engines

The studied model for this current paper, five designs of manifold were considered to study the flow of air behavior. Geometries model of manifolds in this study used the commonly available Computational Fluid Dynamic (CFD) software package FLUENT 6.3. is applied. FLUENT 6.3 has the advantages of importing geometry directly from a Gambit is a software package designed to help in building mesh models for (CFD). The three steps of creating and meshing a geometry using Gambit is as follows:-

- Creating the geometry.
- Meshing the geometry.
- Assigning appropriate zone to the boundaries.

At the beginning, the 3D geometries construct of intake manifolds are built by the Gambit software; as shown in figure (1). The files created by Gambit are imported into FLUENT 6.3 to build mesh for final simulation calculation. Different parameters are considered as well such as the Dean number (Dn) and curvature ratio ( $\gamma$ ). The Dean number is used to provide the measurement of inertial and centrifugal force relative to viscous force through the curve duct. This dimensionless number can be defined as:

$$Dn = Re \sqrt{\frac{D_h}{R_o}} \tag{1}$$

Where:-

$$Re = \frac{\rho u_{in} \cdot D_h}{\mu} \tag{2}$$

$D_h$ : Hydraulic diameter

$R_o$ : bend curvature radius

Curvature ratio ( $\gamma$ ) plays an important role for the study of curved pipe figure (1) .It is defined as an additional parameter characterizing the flow [10].

$$\gamma = \frac{D_h}{R_o} \tag{3}$$

The geometry of the air manifold with total length (2m) and diameter (0.0635m) for duct intake manifold diameter (0.0365m), the experimental work was carried out in the thermodynamics laboratory of mechanical engineering department in the college of engineering, university of Basrah. The laboratory consists of test banks involving (Prodit GR0306/000/013 –variable compression engine

“VARICOMP” dual diesel-petrol cycles) engine, (INFRAGAS - 209) type exhaust gas analyzer for measuring, and support equipment such as Personal Computer (PC) for displaying and saving data as shown in figure (2).

## 3. Computational Analysis

In completing a CFD analysis of the entire domain of the duct, it is necessary to set up the governing equations. For the specific case of flow through the pipe, the governing equations could be solved with the aid of the following assumptions:

1. The flow is steady state.
2. The working fluid is air.
3. The flow is turbulent and incompressible.
4. The duct is at horizontal plane.
5. The properties of flow are constant.
6. The body forces are neglected.
7. The effect of heat transfer is neglected.

According to the previous assumptions the continuity and momentum equations for the turbulent flow in the Cylindrical Coordinates

System  $r$ ,  $\phi$  and  $z$  are written respectively as follows [11]:

**Continuity equation: -**

$$\frac{1}{r} \frac{\partial}{\partial r} (ru) + \frac{1}{r} \frac{\partial}{\partial \phi} (v) + \frac{\partial}{\partial z} (w) = 0 \tag{4}$$

**Momentum equation: -**

$r$ -momentum equation:

$$\rho \left( u \frac{\partial(u)}{\partial r} + v \frac{1}{r} \frac{\partial(u)}{\partial \phi} - \frac{v^2}{r} + w \frac{\partial(u)}{\partial z} \right) = \bar{F}_r - \frac{\partial \bar{P}}{\partial r} + \left[ \frac{1}{r^2} \frac{\partial}{\partial r} \left( r^3 \mu_{eff} \frac{\partial}{\partial r} \left( \frac{u}{r} \right) \right) + \frac{1}{r} \frac{\partial}{\partial \phi} \left( \frac{\mu_{eff}}{r} \frac{\partial u}{\partial \phi} \right) + \frac{\partial}{\partial z} \left( \mu_{eff} \frac{\partial u}{\partial z} \right) - \mu_{eff} \frac{2}{r^2} \frac{\partial v}{\partial \phi} \right] + S_r \tag{5}$$

Where

$$S_r = \frac{1}{r^2} \frac{\partial}{\partial r} \left( r^3 \mu_t \frac{\partial}{\partial r} \left( \frac{u}{r} \right) \right) + \frac{1}{r} \frac{\partial}{\partial \phi} \left( \mu_t r \frac{\partial}{\partial r} \left( \frac{v}{r} \right) \right) + \frac{\partial}{\partial z} \left( \mu_t \frac{\partial w}{\partial z} \right) - \frac{2}{3} \rho \frac{\partial k}{\partial r} \tag{6}$$

momentum equation:

$$\rho \left( u \frac{\partial v}{\partial r} + \frac{v}{r} \frac{\partial v}{\partial \phi} + \frac{uv}{r} + w \frac{\partial v}{\partial z} \right) = \bar{F}_\phi - \frac{1}{r} \frac{\partial \bar{P}}{\partial \phi} + \left[ \frac{1}{r^2} \frac{\partial}{\partial r} \left( r^3 \mu_{eff} \frac{\partial}{\partial r} \left( \frac{v}{r} \right) \right) + \frac{1}{r} \frac{\partial}{\partial \phi} \left( \frac{\mu_{eff}}{r} \frac{\partial v}{\partial \phi} \right) + \frac{\partial}{\partial z} \left( \mu_{eff} \frac{\partial v}{\partial z} \right) + \mu_{eff} \frac{2}{r^2} \frac{\partial u}{\partial \phi} \right] + S_\phi \tag{7}$$

Where

$$S_\phi = \frac{1}{r} \frac{\partial}{\partial \phi} \left( \frac{\mu_t}{r} \frac{\partial v}{\partial \phi} \right) + \frac{2}{r} \frac{\partial}{\partial \phi} \left( \mu_t \frac{u}{r} \right) + \frac{\partial}{\partial r} \left( \frac{\mu_t}{r} \frac{\partial u}{\partial \phi} \right) + \frac{\partial}{\partial z} \left( \frac{\mu_t}{r} \frac{\partial w}{\partial \phi} \right) - \frac{2}{3} \frac{\rho}{r} \frac{\partial k}{\partial \phi} \quad (8)$$

z-momentum equation:

$$\rho \left( u \frac{\partial w}{\partial r} + \frac{v}{r} \frac{\partial w}{\partial \phi} + w \frac{\partial w}{\partial z} \right) = \bar{F}_z - \frac{\partial \bar{P}}{\partial z} + \left[ \frac{1}{r} \frac{\partial}{\partial r} \left( r \mu_{eff} \frac{\partial w}{\partial r} \right) + \frac{1}{r} \frac{\partial}{\partial \phi} \left( \frac{\mu_{eff}}{r} \frac{\partial w}{\partial \phi} \right) \right] \text{ Where} \quad (9)$$

$$+ \frac{\partial}{\partial z} \left( \mu_{eff} \frac{\partial w}{\partial z} \right) + S_z$$

$$S_z = \frac{1}{r} \frac{\partial}{\partial r} \left( \mu_t r \frac{\partial u}{\partial z} \right) + \frac{1}{r} \frac{\partial}{\partial \phi} \left( \mu_t \frac{\partial v}{\partial z} \right) + \frac{\partial}{\partial z} \left( \mu_t \frac{\partial w}{\partial z} \right) - \frac{2}{3} \rho \frac{\partial k}{\partial z} \quad (10)$$

### 3.1. The standard k-ε model

The standard k-ε model has two model equations one for k and one for ε. The standard model uses the following transport equations for k and ε [11].

$$\mu_t = \frac{C_\mu \rho k^2}{\varepsilon} \quad (11)$$

$$\rho \left( u \frac{\partial k}{\partial r} + \frac{v}{r} \frac{\partial k}{\partial \phi} + w \frac{\partial k}{\partial z} \right) = \left[ \frac{1}{r} \frac{\partial}{\partial r} \left( r \frac{\mu_t}{\sigma_k} \frac{\partial k}{\partial r} \right) + \frac{1}{r} \frac{\partial}{\partial \phi} \left( \frac{\mu_t}{\sigma_k} \frac{\partial k}{\partial \phi} \right) + \frac{\partial}{\partial z} \left( \frac{\mu_t}{\sigma_k} \frac{\partial k}{\partial z} \right) \right] + G - \rho \varepsilon \quad (12)$$

$$\rho \left( u \frac{\partial \varepsilon}{\partial r} + \frac{v}{r} \frac{\partial \varepsilon}{\partial \phi} + w \frac{\partial \varepsilon}{\partial z} \right) = \left[ \frac{1}{r} \frac{\partial}{\partial r} \left( r \frac{\mu_t}{\sigma_\varepsilon} \frac{\partial \varepsilon}{\partial r} \right) + \frac{1}{r} \frac{\partial}{\partial \phi} \left( \frac{\mu_t}{\sigma_\varepsilon} \frac{\partial \varepsilon}{\partial \phi} \right) + \frac{\partial}{\partial z} \left( \frac{\mu_t}{\sigma_\varepsilon} \frac{\partial \varepsilon}{\partial z} \right) \right] + C_{\varepsilon 1} \frac{\varepsilon}{k} G - C_{\varepsilon 2} \rho \frac{\varepsilon^2}{k} \quad (13)$$

$$G = \mu_t \left\{ 2 \left[ \left( \frac{\partial u}{\partial r} \right)^2 + \left( \frac{1}{r} \frac{\partial v}{\partial \phi} \right)^2 + \left( \frac{\partial w}{\partial z} \right)^2 \right] + \left( \frac{1}{r} \frac{\partial w}{\partial \phi} + \frac{\partial v}{\partial z} \right)^2 + \left( \frac{\partial u}{\partial z} + \frac{\partial w}{\partial r} \right)^2 + \left( \frac{1}{r} \frac{\partial u}{\partial \phi} + \frac{\partial v}{\partial r} - \frac{v}{r} \right)^2 \right\} \quad (14)$$

Where G: Turbulent production term of kinetic energy.

Table (1) empirical constants in the k-ε

$C_\mu$	$C_{1\varepsilon}$	$C_{2\varepsilon}$	$\sigma_k$	$\sigma_\varepsilon$
0.09	1.44	1.92	1.00	1.30

## 3.2 Boundary conditions

### 3.2.1 Boundary conditions at the inlet

$$\left. \begin{aligned} u = v = 0 \\ w = w_{in} \end{aligned} \right\} \quad (15)$$

$$\left. \begin{aligned} k_{in} = C_k w_{in}^2 \\ \varepsilon_{in} = C_\mu k_{in}^{3/2} / (0.5 D_h C_\varepsilon) \end{aligned} \right\} \quad (16)$$

Where

$D_h$ : Hydraulic diameter

( $C_k=0.003$  &  $C_\varepsilon=0.03$ ) [11].

### 3.2.2 Boundary conditions at the outlet

The outlet pressure is zero.

$$\frac{\partial u}{\partial z} = \frac{\partial v}{\partial z} = \frac{\partial w}{\partial z} = 0 \quad (17)$$

$$\frac{\partial k}{\partial z} = \frac{\partial \varepsilon}{\partial z} = 0 \quad (18)$$

### 3.2.3 Boundary conditions at the solid boundaries

No slip boundary condition is applied to all of the wall surfaces. Velocity components (u, v, and w): In the present study the solid surfaces are stationary so the velocity components (u, v, and w) are set to zero [11], the k and ε at the region near walls are:

$$k_p = \frac{\tau_w}{\rho C_\mu^{1/2}} \quad (19)$$

$$\varepsilon_p = \frac{C_\mu^{3/4} k_p^{3/2}}{K y_p} \quad (20)$$

$K_i$ : Turbulent kinetic energy at point near wall,  $\tau_w$ : Wall shear stress &

$\varepsilon_p$ : Dissipation rate of turbulent kinetic energy at point near wall.

## 4. Results & Discussions

### 4.1. Theoretical results

This part includes the details of computational results for the hydrodynamic characteristics of the turbulent flow through the five cases of the engine manifold. The effects of various parameters (velocity, static pressure, swirl and tumble inside the manifold and cylinder) on the engine performance will be introduced, to show the changing into motion inside the engine cylinder along multi planes as describe in figure (3) (at the end of manifold plane (A-A), plane and longitudinal section in the cylinder (B-B) cross-section in the cylinder

(C-C) plane) at as shown in figure (3). The physical model is studied schematically in figure (3) as the one case from

the five cases of manifold and the engine cylinder at the end of the suction stroke (BDC).

#### 4.1.1 Effect of curvature ratio

The fluid trajectory vectors support the influence of the manifold design configuration on the overall flow in the cylinder. In the non-optimized manifold, these vectors present stirring motions that hinder the flow and cylinder filling. When entering inside the cylinder, the fluid trajectories, in the optimized manifold, form circulating swirl movements, which further enhances the filling and combustion process. As a conclusion, the distributions of the velocity fields and the air fuel mixture are strongly depending on the intake manifold geometry.

The effect of bent pipe with different curvature ratios ( $\gamma$ ) on the flow behavior has been illustrated in figures (4 to 8) at constant inlet velocity flow see table 2.

Table (2) curvature ratio effect at 3000 RPM

Case	Reynolds number (Re)	Dean number (Dn)	Curvature ratios ( $\gamma$ )
Case (1)	6261.82142	0	0
Case (2)	6403.52411	319.40778	0.04988
Case (3)	6261.82142	624.24098	0.09969
Case (4)	6097.03704	1217.51733	0.19969
Case (5)	5037.94322	2295.86609	0.14978

Figure (4) shows the effect of curvature ratio on the distribution of tangential velocity  $v$  (with  $\phi$ - direction) at the end of manifold plane (A-A) with different manifold cases 1, 2, 3, 4 and 5. Velocity distribution with  $\phi$ -direction due to the centrifugal forces induced by the curvature tends to push the fluid in the core region toward the outer wall of the bend. These forces turn move the fluid around the outer wall back toward the inner wall along the side walls forming a pair vortex. The length and orientation of each vector are determined by the magnitude and direction of the in-plane velocity characterizing the secondary flow. In addition, each vector is color-coded according to the magnitude of the full three-dimensional velocity, as shown by the color bar. Thus the secondary flow consists of two vortex flows of opposite sign: a counterclockwise circulation in the top half, accompanied by a clockwise circulation in the bottom half of the velocity vectors that were displayed. Meanwhile, the fluid near the upper and lower walls is forced inwardly along the walls by the vivid secondary flow. From figure (4) has appeared secondary flow due to the tangential velocity flow when the curvature ratios increased as in case 5, case 3 and case 2 respectively secondary flows is a greater effected than cases 1 and 4.

Figure (5) indicates velocity magnitude vector at the cross section plane of manifold, (plane B-B) that swirl and tumble flow inside the cylinder are highly appeared at a different curvature ratio. To explain the swirl motion inside the cylinder, plane (C-C) is created.

Distributions of the longitudinal and circumferential velocity components in the vertical and horizontal plane are shown clearly on the intake port and cylinder. At the beginning region of the manifold a uniform flow with all curvature ratio values has appeared. While at the bent region near the engine valve the velocity magnitude is

increased due to the bent and the restriction part. Gas blend is drawn by the downward motion of the piston. The mixture spreads in the cylinder and interacts with cylinder walls. When the flow reaches the inlet valve, it undergoes an acceleration considering the valve restriction surface the air movement is in a very complex flow condition especially near the valve seat. The fluid flows at this region are nearly reached to 5.31 m/s at case 1 passing through the valve, 5.1 m/s at case 2, 5.366 m/s at case 3, 5.229 m/s at case 4 and 5.1 m/s at case 5. These results show the effect of curvature ratio on the flow velocity as swirl and tumble. Where swirl is a radial velocity and tumble is a tangential velocity. High velocity flow is illustrated around the valve while low velocity under the valve which creates, the Swirl and tumble flow to increase the air-fuel mixture. The mixture flow can be visualized by the velocity distribution in the intake port and the cylinder is shown in the figure 5. From this figure the plane (B-B), the large scale tumble swirl is formed by the mixture the flow through the intake valve, and the tumble swirl will be kept until the end of the compression stroke, the vortex is produced under the valve. In plane (C-C) the secondary flow develops into a pairs of vortices.

To show the fluid flow u-velocity at the end of the manifold plane (A-A) at line (1), figure (6) was plotted with different curvature ratios and constant inlet velocity. From this figure it can be seen that the velocity increases toward the outer wall when the curvature ratio ( $\gamma$ ) increases due to increase the centrifugal force. In other words the secondary flow is a maximum in the high angle of the pipe.

In figure (7) at the end of manifold plane (A-A) at line (1) represents the distribution of static pressure across the diameter, at the center of pipe for different curvature ratios (five cases). This figure shows that the static pressure increases at inner wall in case 5, case 3 and case 2 because the centrifugal force on the fluid increases due to its curved trajectory. When the curvature ratio is increased it created pressure difference along the radius as case 5, case3 and case 2 respectively in figure (7).

The static pressure contour at the plane (B-B) for cases 5 is illustrated in figures (8) at engine speed 3000 RPM. The regions of the low pressure increase with increasing  $\gamma$  at the inside of the engine cylinder because the mixture flow enters the cylinder with high turbulence. When the regions of the vacuum pressure increase air is being quite freely admitted to the engine, which in turn means that more air and fuel is being provided to it, which generates more power. This enhances its capability of carrying fuel droplets and increases evaporation and air-fuel mixing. From figure case (5) is optimized the intake manifold because vacuum pressure in these case greater than vacuum pressure in other cases. High vacuum pressure in the cylinder helps the combustion to occur very efficiently because the high vacuum pressure is aid evaporate fuel.

#### 4.2. Experimental results

Test results for each case performed are recorded by measuring the engine performance, exhaust gas concentrations and relative air/fuel ratio ( $\lambda$ ). They are taken at engine speeds (1000, 1500, 2000, 2500, 3000 and 3500

RPM) respectively. Lambda ( $\lambda$ ) is defined as actual AFR to the ideal or stoichiometric of AFR. Lambda for optimum emissions, fuel economy, and good engine performance is around 1.

Figure (9) plots the fuel consumption  $Q_{vf}$  (l/h) versus engine speed at  $Cr = 10$  for all cases, were plotted. The fuel consumption of the engine increases with increasing engine speed, due to the higher flow rate of air will create an even lower pressure in the venture throat. This creates a greater pressure differential through the fuel capillary tube, which increases the fuel flow rate to keep up with the greater air flow rate and engine demand. From the figure it is seen for case (5) that intake manifold is optimized because it has smaller  $Q_{vf}$  at high engine speed due to high air swirl which increase the mixture strength.

Figure (10), presents the amount of hydrocarbon concentrations in an exhaust gases with different engine speed, manifold design and constant compression ratio. The results show acceptable value of  $HC$  at low engine speed due to enhance air-fuel mixture at the ideal speed. The unburned fuel was appeared when engine speed increased to 1500 RPM due to sudden increased of engine speed and creates the rich mixture (unburned fuel). At all engine speed the results show minimum unburned fuel when using the case (5) especially at high engine speed that means correct combustion is happened with new manifold.

Figure (11), shows oxygen ( $O_2$ ) concentrations variation with engine speed at  $Cr = 10$  for all cases. Oxygen ( $O_2$ ) concentrations increase as engine speed decreases because it increases the volumetric efficiency for all cases. At (1000 RPM) ( $O_2$ ) is maximum and at (1000 to 3500 RPM) is decreases gradually. As mixture goes rich of stoichiometry, oxygen falls close to zero. Because oxygen is used up in the combustion process, concentrations at the tailpipe will be very low. If misfire occurs, however, oxygen will increase dramatically as it passes unused through the combustion chamber. At (1000 RPM), more air can enter causing higher concentrations of  $O_2$  in the exhaust, because of the high volumetric efficiency. As engine speed increases no more air can enter through causing lower concentrations of  $O_2$  in the exhaust, because most of the available oxygen is consumed in the combustion process. At all engine speed the results show minimum oxygen when using the case (5) that means correct combustion is happened with this manifold.

Figure (12), presents the relative air fuel ratio ( $\lambda$ ) with different engine speed, engine manifold cases (1, 2, 3, 4 and 5) and  $Cr$  (10) were plotted. At (1000 RPM) ( $\lambda$ ) is maximum because of the high volumetric efficiency. At 1500-2500 it is minimum because the mixture is rich and from 2500 to 3500 RPM it increases gradually because at high air velocity and turbulence, this enhances its capability of carrying fuel droplets and increases evaporation and air-fuel mixing. Good approach between the five cases is shown in case 5 (135°-NE).  $\lambda$  values depend on exhaust gas

concentrations and were calculated from Brettschneider equation (21), see figure (13) [12].

$$\lambda = \frac{\left( [CO_2] + \frac{[CO]}{2} + \frac{[NO_2]}{2} + [O_2] + \left( \frac{H_{cv}}{4} \left( \frac{3.5}{3.5 + \frac{[CO]}{[CO_2]}} \right) - \frac{O_{cv}}{2} \right) ([CO_2] + [CO]) \right)}{\left( \left( 1 + \frac{H_{cv}}{4} - \frac{O_{cv}}{2} \right) ([CO_2] + [CO] + [HC]) \right)} \quad \text{---(21)}$$

Where

$H_{cv}$  : Atomic ratio of hydrogen to carbon in the fuel &  $O_{cv}$  : Atomic ratio of Oxygen to Carbon in the fuel.

## 5. Conclusions

The most important conclusions that can be drawn from the present study are as the following:

- 1- The analysis of the flow during the intake stroke is numerically made by a CFD code. The numerical study made it possible to select the optimum intake system geometry.
- 2- Velocity and pressure field are investigated in this simulation, the results affirm that the optimum manifold can be obtained numerically.
- 3- Velocity is highest near the outer wall at increased the curvature ratio and pressure is highest near the inner wall at increased the curvature ratio.
- 4- The distributions of the velocity fields and the air fuel mixture are strongly depending on the engine speed and intake manifold geometry.
- 5- Investigated experimentally the optimized manifold (case 5) due to enhance AFR, fuel consumption and exhaust emissions are improved.
- 6- Numerical and experimental results showed that the great impact of the intake manifold on the fuel mixture formation and engine speeds.
- 7- Ability of the curved pipe on the fluid mixing enhancement due to the secondary flow, the secondary flow give the excess performance and exhaust emissions due fluid mixing properties.

## 6. Reference

- [1] Vadivel P. and Vamsidhar D., "Computational Analysis Of Intake Manifold Design And Experimental Investigation On Diesel Engine For LCV", CFD Department, Defiance Technologies Chennai, Tamil Nadu, India, Vol. 3 No. 4 Mar 2011.
- [2] Jemni, M. A., Kantchev, G., And Abid, M. S., "Intake manifold design effect on air fuel mixing and flow for an LPG heavy duty engine", International journal of energy and environment Vol. 3, Issue 1, 2012 pp.61-72.
- [3] Heywood, J.B., "Internal combustion engine fundamentals", McGraw-Hill Inc, Inc., New York, (1988).
- [4] Mark, C., And Donald, H., "Improvement of Intake Restrictor Performance for a Formula SAE Race Car through 1D & Coupled 1D/3D Analysis Methods", University of Minnesota, 2006-01-3654.
- [5] Ramasamy, D., Zamri, M., Mahendran, S., And Vijayan S., "Design Optimization of Air Intake System (AIS) of 1.6L Engine by Adding Guide Vane", IMECS 2010.

- [6] Hongjiang, CUI, “**The Steady Flow Test and CFD Numerical Simulation on Improving Research of Locomotive Diesel Engine Helical Intake Port**”, 2010 WASE International Conference on Information Engineering.
- [7] Jianqin, F., “**A Method for Designing and Studying Engine Intake System Based on CAD/CAE/CFD Integration**”, Research Center for Advanced Powertrain Technology, Hunan University, Changsha, Hunan 410082, China, 2011.
- [8] Liu, S., “**Analog Computation and Experimental Study of Small Gasoline Engine**”, School of automobile and traffic engineering Jiangsu University, IEEE 2011.
- [9] Wes, M. M. And Abood, M. H., “**Study Of Inlet Mixture Temperature Influence On The Spark Ignition Engine Performance And Exhaust Emissions**”, Karbala university, 2010.
- [10] Nawar, S. S., “**Three Dimensional Numerical Study of Heat Transfer Enhancement Through a Flow Inside Curved Duct**”, The College of Engineering University of Basra, M.Sc. Thesis, 2012.
- [11] Salman, A. M., “**Turbulent Forced Convection Heat Transfer in the Developing Flow through Concentric Annuli**”, Mechanical engineering department of university of Technology, M.Sc. Thesis, July 2003.
- [12] Toyota Company, “**Combustion Chemistry & Emission Analysis**”, Advanced Emissions & Driveability Diagnosis Technical Training - Course 972, Toyota Motor Sales USA, Inc.

**Nomenclature**  
**English Symbols**

Symbol	Definition	SI Units
$C_{\mu}, C_{1\varepsilon}, C_{2\varepsilon}$	Constants in turbulence model	—
Cr	Compression ratio	—
$D_h$	Hydraulic diameter	m
$D_n$	Dean number, $Re \left( \frac{D_h}{R_o} \right)^{1/2}$	—
$F_r, F_{\phi}, F_z$	Body force	N/m <sup>3</sup>
$H_{cv}$	Atomic ratio of hydrogen to carbon in the fuel	—
k	Turbulent kinetic energy = $\frac{1}{2} (\overline{u'^2} + \overline{v'^2} + \overline{w'^2})$	m <sup>2</sup> /s <sup>2</sup>
$k_p$	Turbulent kinetic energy at point near wall	m <sup>2</sup> /s <sup>2</sup>
m	Mass	kg
NP	Near the plenum	—
NE	Near the engine	—
$O_{cv}$	Atomic ratio of Oxygen to Carbon in the fuel	—
p	Pressure	N/m <sup>2</sup>
$Q_{vf}$	Fuel consumption	l/h
Re	Reynolds number = $\rho u_{in} D_h / \mu$	—
$R_o$	Radius of curvature	m
Sr, S $\phi$ and Sz	Source term	N/m <sup>3</sup>
$u, v, w$	velocities in r, $\phi$ and z direction	m/s
$u_{in}$	Average inlet velocity	m/s
r, $\phi$ and z	Cylindrical coordinates	m

**Greek Symbols**

Symbols	Definition	SI Units
$\gamma$	Curvature ratio, = $D_h / R_o$	—
$\varepsilon$	Dissipation rate of turbulent kinetic energy	m <sup>2</sup> /s <sup>2</sup>
$\varepsilon_p$	Dissipation rate of turbulent kinetic energy at point near wall	m <sup>2</sup> /s <sup>2</sup>
$\theta$	Axial direction	—
$\lambda$	Normalized AFR, $\lambda = \frac{AFR_{act.}}{AFR_{stoich.}}$	—
$\mu_{eff}$	Effective viscosity	N. s/m <sup>2</sup>
$\nu$	Kinematic viscosity	m <sup>2</sup> /s
$\rho$	Density of air	kg/m <sup>3</sup>
$\sigma_k, \sigma_{\varepsilon}$	Turbulent Prandtl numbers for k, $\varepsilon$	—
$\tau_w$	Shear stress	N/m <sup>2</sup>

**Subscripts**

<b>Symbol</b>	<b>Definition</b>
Act.	Actual value
eff	Effective
in	Inlet
out	Outlet
r	Radial direction
Stoch.	Stoichometric value
z	Axial direction

**Group Abbreviations**

<b>Symbol</b>	<b>Definition</b>
AFR	Air to fuel ratio
BTDC	Bottom and top dead center
<i>CFD</i>	Computational fluid dynamics
CAD	Computer aided design
CAE	Computer aided engineering
GAMBIT	Package softwere
IC	Internal combustion
IM	Inlet manifold
$k-\varepsilon$	turbulence model
ppm	Part per million
PDE	Partial differential equation
RPM	Revolution per minute
SIMPLE	Semi-implicit method for pressure-linked equations
SI	Spark-ignition engines

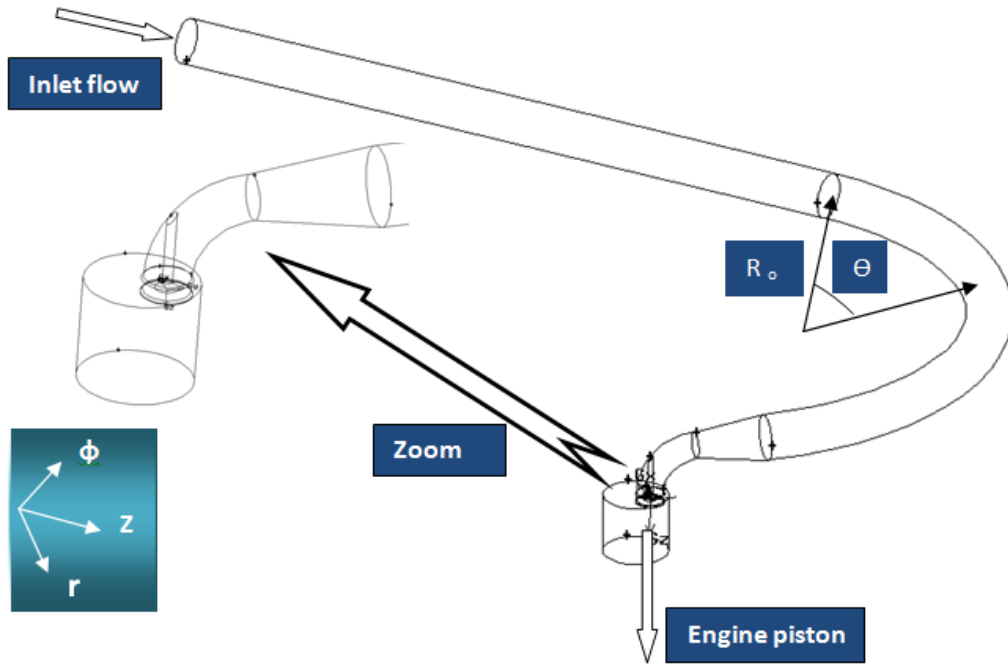


Fig. 1 Intake manifold and cylinder

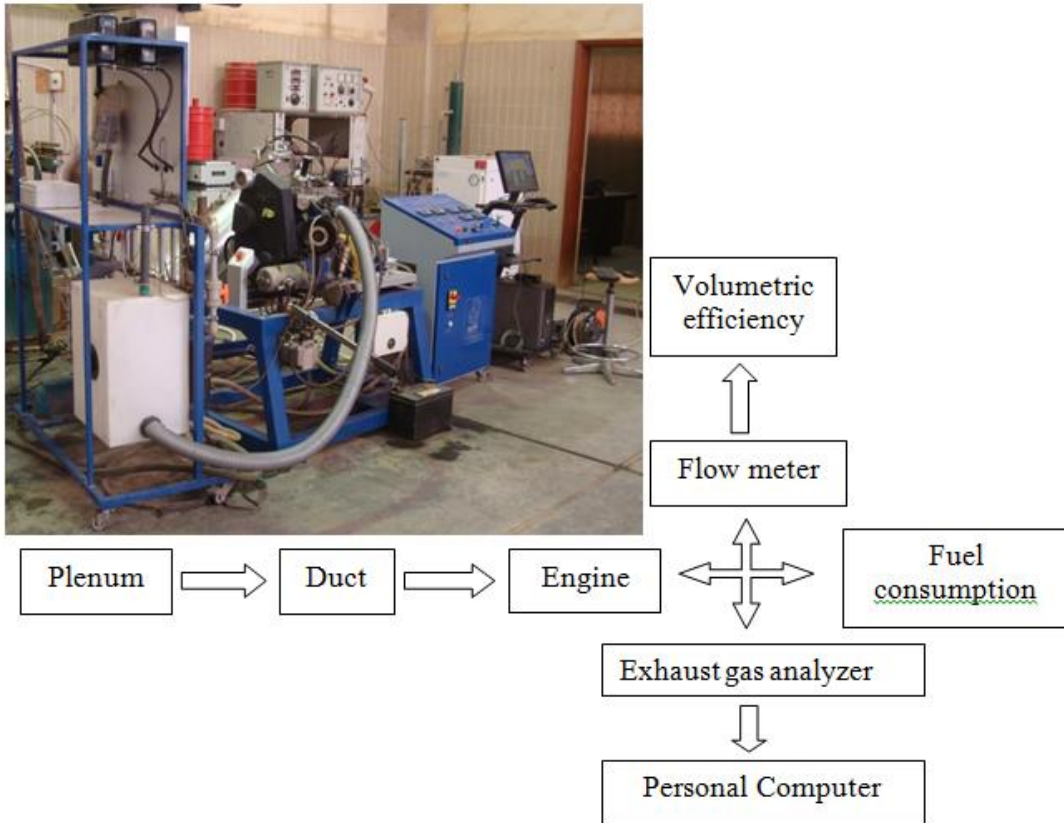


Fig. 2 Test equipment's photograph

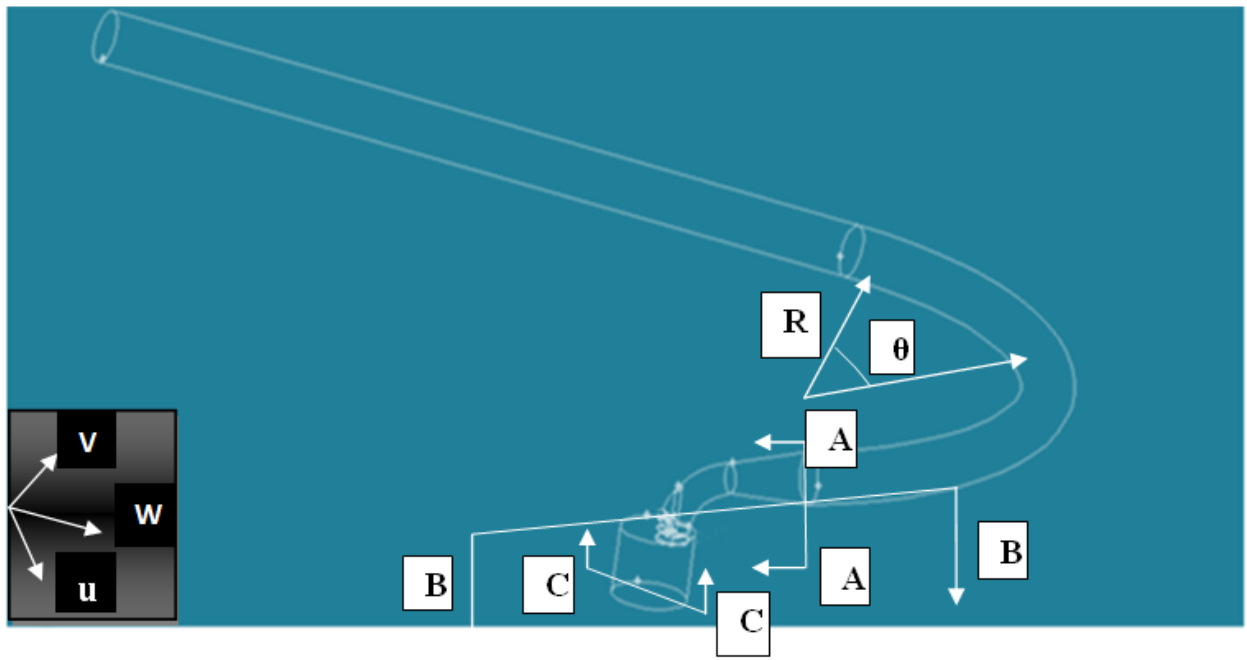


Fig. 3 The physical model at BDC

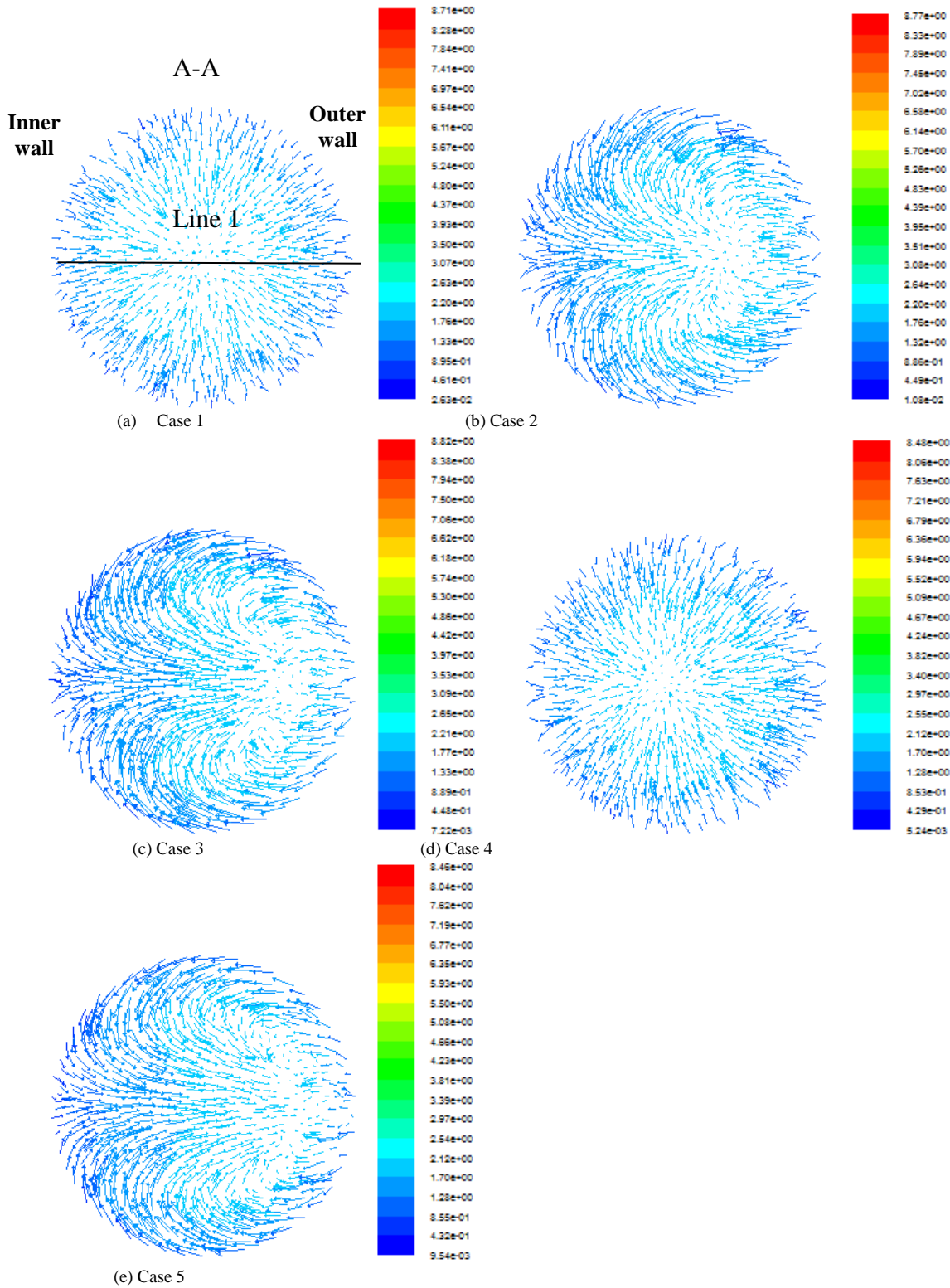
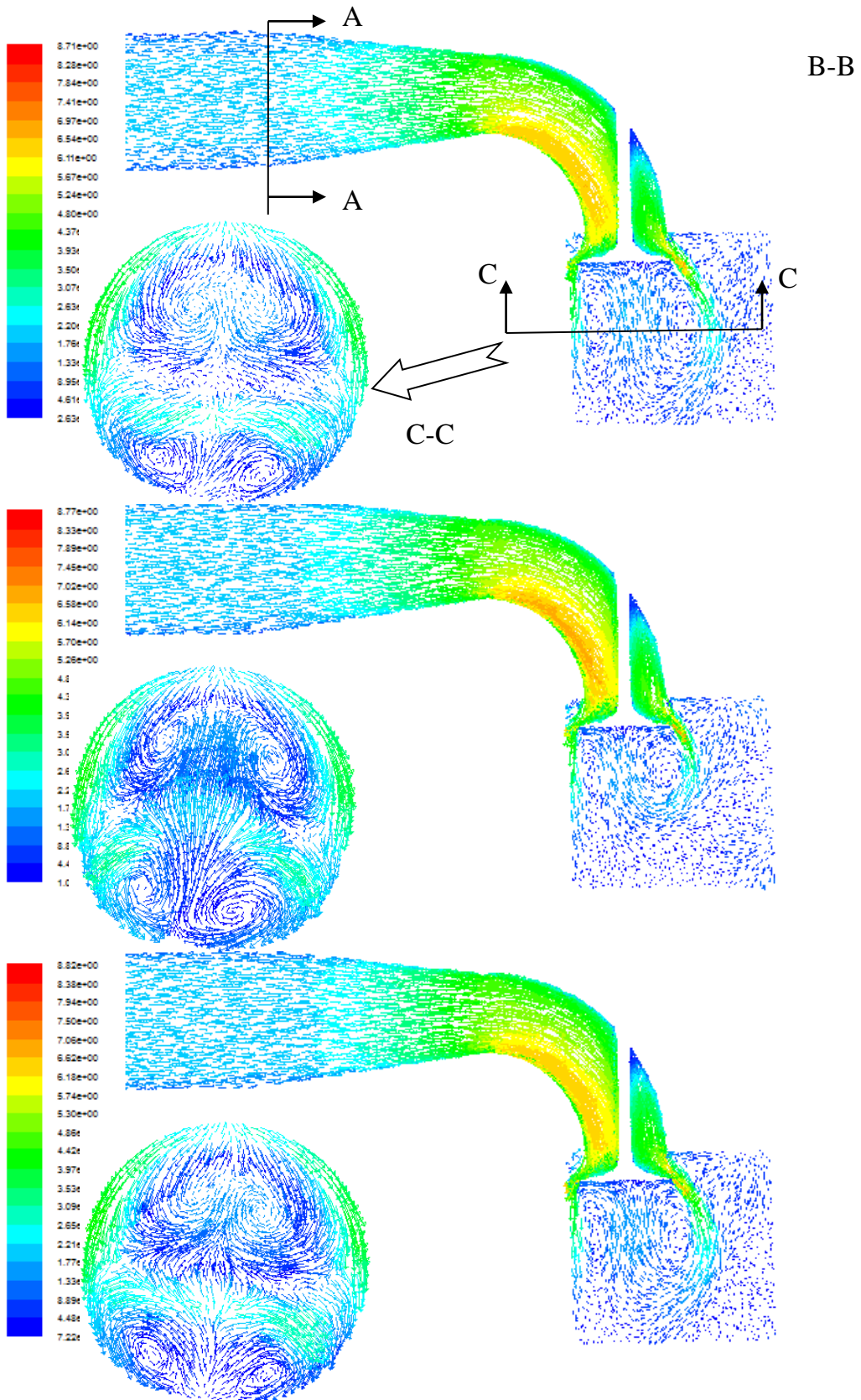
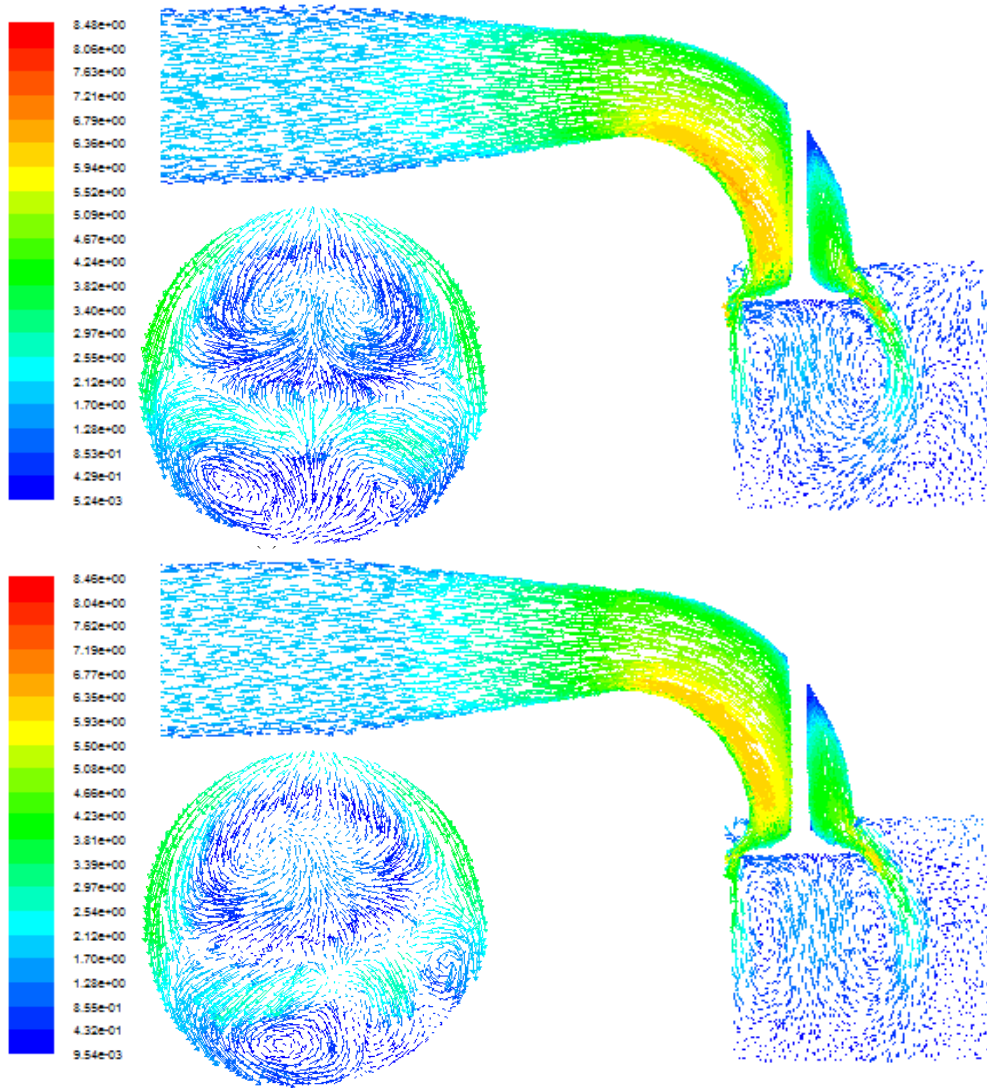


Fig. 4 Tangential flow v-velocity vectors at plane (A-A) of flow through cases 1, 2, 3, 4 and 5 at 3000 RPM and piston at BDC





(e) Case 5  
Fig. 5 Velocity vectors at two planes (B-B) and (C-C) of flow through cases 1, 2, 3, 4 and 5 at 3000 RPM and piston at BDC

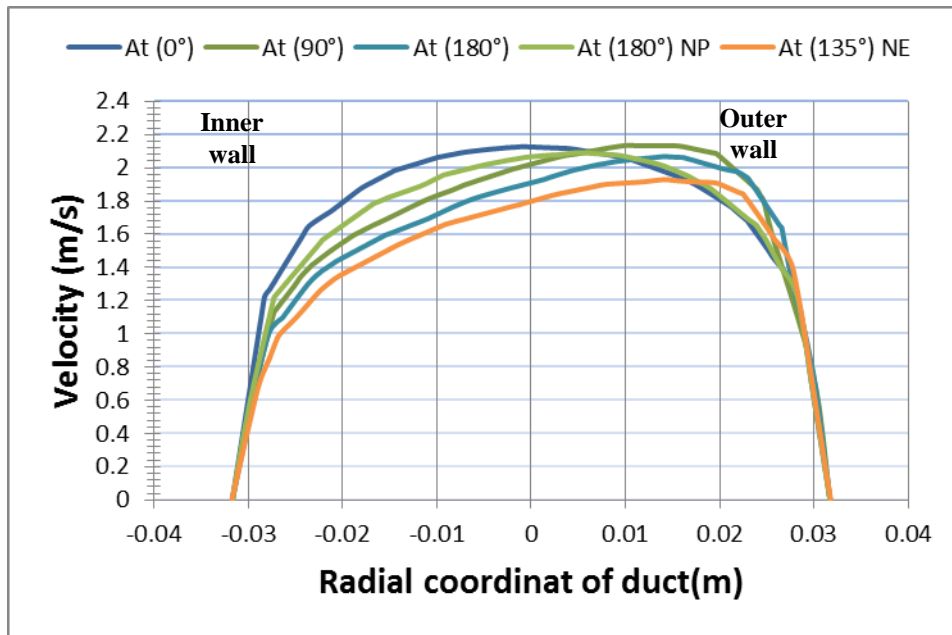


Fig. 6 Velocity magnitude at line (1) in (A-A) plane for cases 1, 2, 3, 4 and 5 at (3000 RPM), Cr (10) and piston at BDC

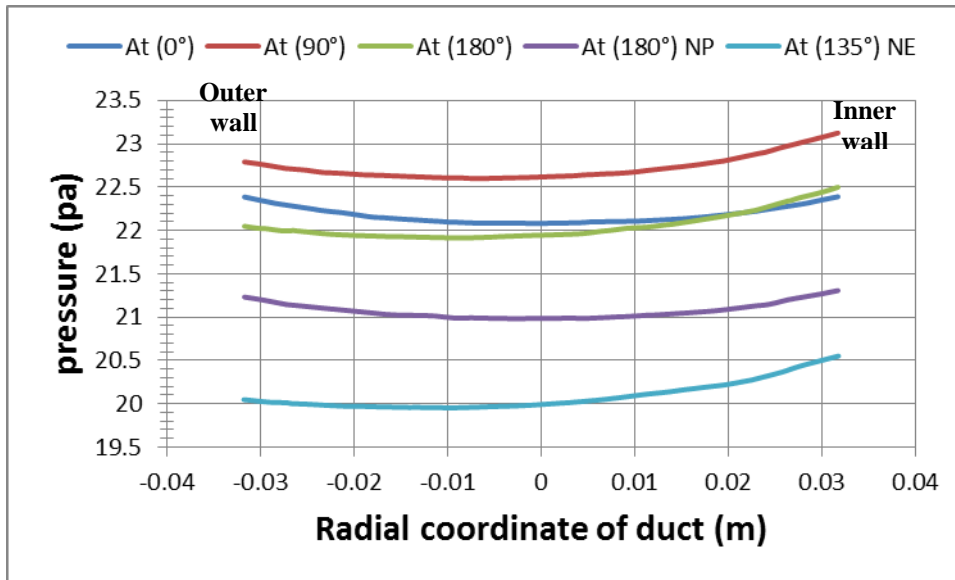


Fig. 7 Static pressure at line (1) in (A-A) plane for cases 1, 2, 3, 4 and 5 at (3000 RPM), Cr (10) and piston at BDC

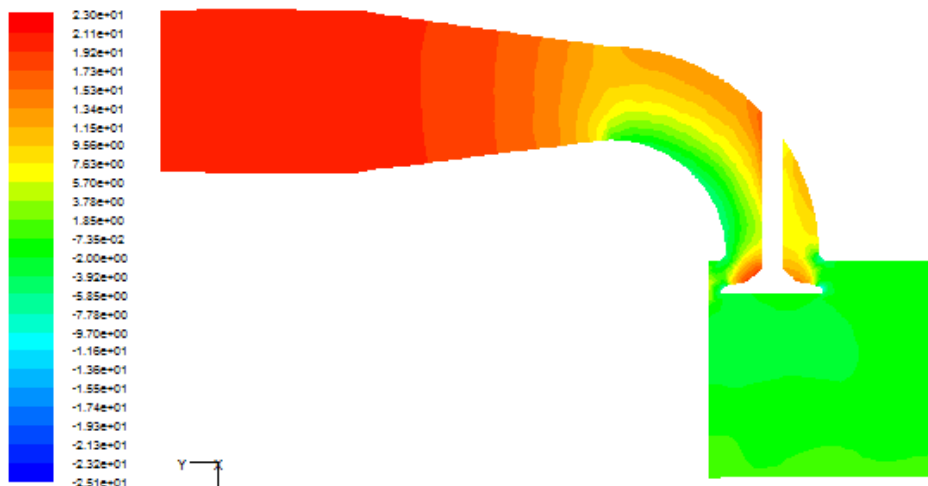


Fig. 8 Contours of static pressure (pa) of flow through cases 5 at 3000 RPM and piston at BDC

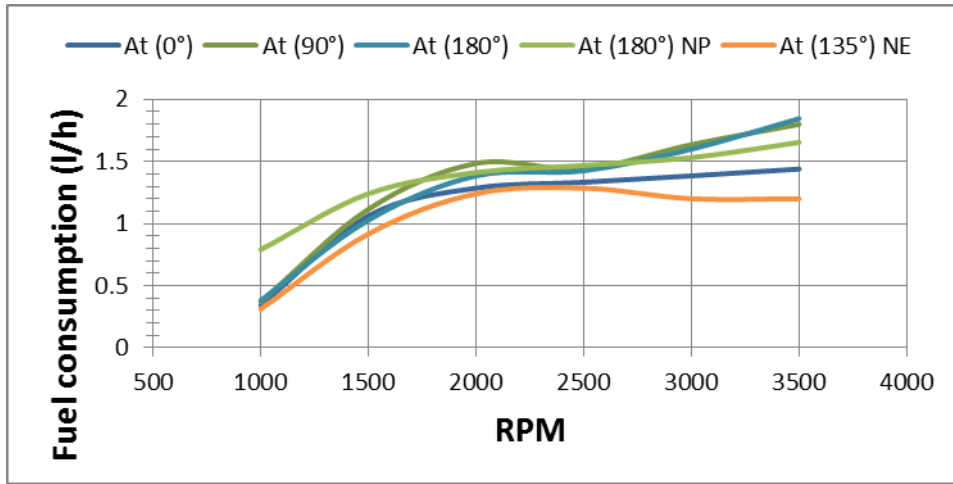


Fig. 9 Fuel consumption ( $Q_{vf}$ (l/h)) for cases 1, 2, 3, 4 and 5 for Cr:10

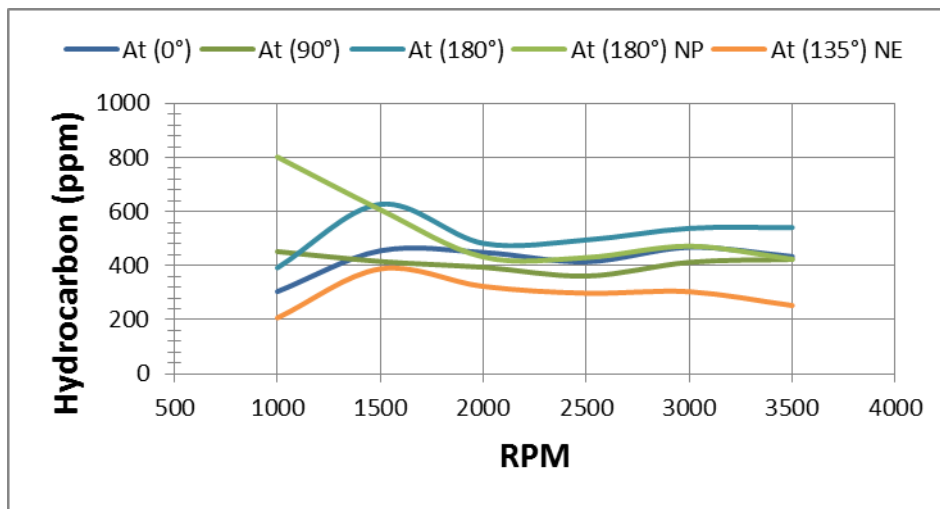


Fig. 10 Hydrocarbon (HC (ppm)) for cases 1, 2, 3, 4 and 5 for Cr:10

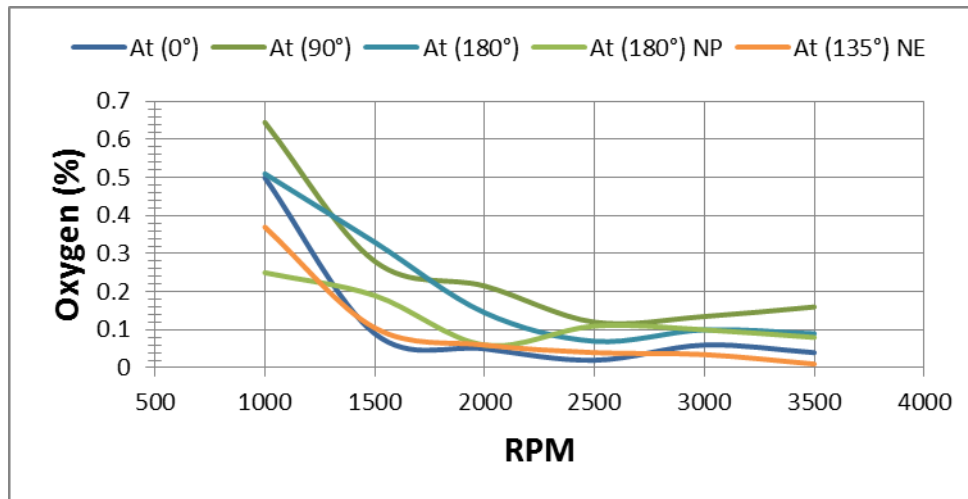


Fig. 11 Oxygen ( $O_2$  (%)) for cases 1, 2, 3, 4 and 5 for Cr:10

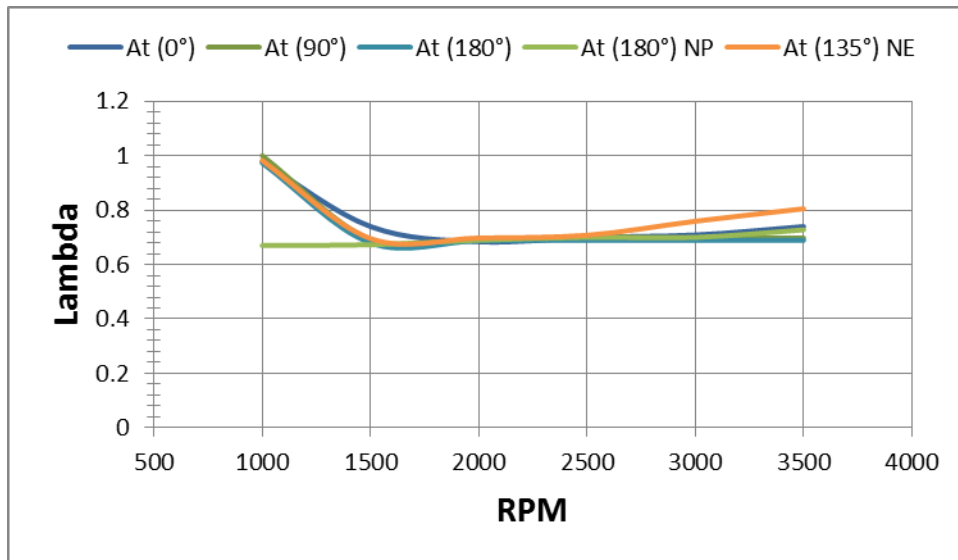


Fig. 12 relative air/fuel ratio, Lambda ( $\lambda$ ) for cases 1, 2, 3, 4 and 5 for Cr:10

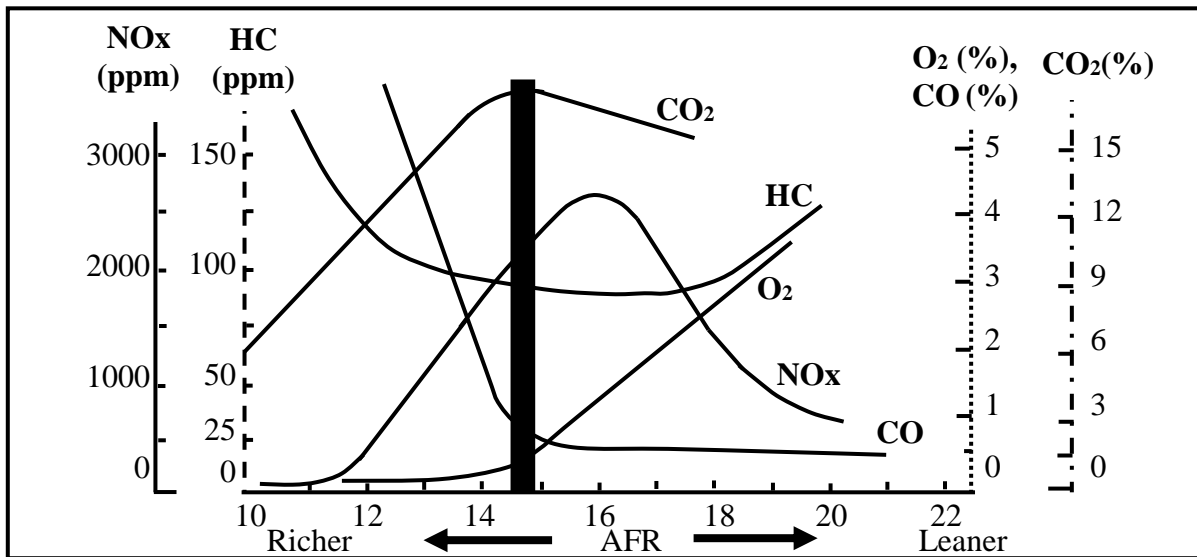


Fig. 13 The effect of AFR on exhaust gases [12]